ACS APPLIED MATERIALS & INTERFACES

Research Article

www.acsami.org

Fabrication of Single-Hole Glutathione-Responsive Degradable Hollow Silica Nanoparticles for Drug Delivery

Dongdong Wang,[†] Zhigang Xu,[†] Zhenjie Chen,[‡] Xiaoyan Liu,[†] Cuilan Hou,[‡] Xiaoyu Zhang,[‡] and Haixia Zhang*,[†]

[†]State Key Laboratory of Applied Organic Chemistry and [‡]Institute of Physiology, School of Basic Medical Sciences, Lanzhou University, Lanzhou 730000, China

Supporting Information

ABSTRACT: In the present study, a kind of single-hole glutathione (GSH)-responsive degradable hollow silica nanoparticles (G-DHSNs) was synthesized and used as carriers of doxorubicin (DOX) (DOX-G-DHSNs). The G-DHSNs were accurately designed and fabricated with a simple and convenient method, and without any extra pernicious component. The composition, morphology and properties of the G-DHSNs had been characterized by ^{1}HNMR spectra, Fourier transform infrared spectrograph, thermo gravimetric analysis, transmission electron microscope, and scanning electron microscope. The degradation study of G-DHSNs showed that the G-DHSNs would be broken into pieces after interacting with GSH. Besides, the negligible hemolytic activity and low cytotoxicity of the G-DHSNs demonstrated its excellent biocompatibility. pH- and GSH-triggered release of DOX followed by the decomposition of G-DHSNs within TCA8113 cancer cells was further confirmed by flow cytometry and confocal laser scanning microscopy studies. All of these results indicated that G-DHSNs can be used as safe and promising drug nanocarriers.

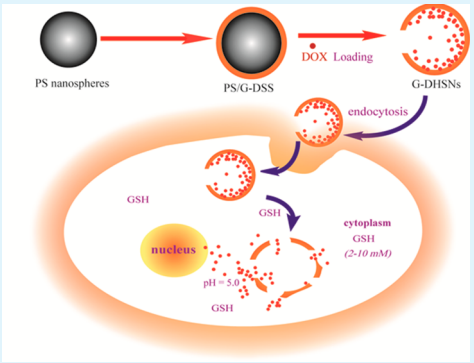

KEYWORDS: *hollow silica nanoparticles, glutathione, drug delivery, cancer therapy*

1. INTRODUCTION

During the past few years, remarkable improvement had been made in the research of drug delivery systems (DDS) for their great potential to cure cancers,[1] which was attributed partly to the developments in nanotechnology involving the fabrication of different structures with attractive functions for DDS. A variety of nanoplatforms, such as silica nanoparticles,[2−5] polymer nanoparticles,[6−8] semiconductor nanocrystals,[9] gold nanoparticles,[10−12] superparamagnetic iron oxide nanoparticles,[13,14] and graphene[15−17] were actively developed for drug delivery. As we all know, nanoparticle-based DDS tended to have increased accumulation in tumors through the leaky tumor neovasculature by the enhanced permeability and retention effect (EPR), known as the passive targeting,[18,19] which decreased the side effects of drugs on normal tissues greatly. The efficient and safe drug delivery vectors were always the research aim for drug therapy. However, poor stability,[20−22] limited drug loading[23] and the cytotoxicity[24,25] remained prohibitive for practical applications of nanoparticle-based DDS.

Silica was generally recognized as safe by the US Food and Drug Administration (FDA), silica nanoparticles, especially hollow silica nanoparticles (HSNs), with high pore volumes, low density, excellent stability, easy functionalization and significant biocompatibility, had gained much attention for their biological and medical applications.[26−31] Efforts had been made to demonstrate that HSNs were efficient carriers for various therapeutic agents. Zink et al.[32] reported three simple and new pH-responsive supramolecular nanovalves on both hollow and conventional mesoporous silica. The authors found that mesoporous HSNs released double times more drug molecules than did conventional HSNs. Leventis et al.[33] evaluated in detail the biocompatibility of a new material of dysprosia aerogel and compared the results with the ordered mesoporous silica. The results showed that the ordered mesoporous silica had accepted biocompatibility too. Tang et al.[34] used mesoporous HSNs as DDS via cell and animal experiments to examine their cytotoxicity and the effect of disease therapy. The clinical features, mortality, pathological examinations and blood biochemical indexes revealed the mesoporous HSNs had low toxicity after injected with the repeated doses. Lin et al.[35] synthesized a kind of MCM-41 mesoporous silica nanosphere-based DDS, in which they used surface-derivatized and cytotoxic cadmium sulfide (CdS) nanocrystals[36,37] as chemically removable caps to encapsulate drugs. To be successful, HSNs usually needed to be functionalized with additional modifications to control the delivery of the bioactive drugs.[27−29,31,38] The complicated and cumbersome fabrication of HSNs DDS hindered the wide use

Received: April 29, 2014
Accepted: July 3, 2014
Published: July 3, 2014

Scheme 1. Schematic Illustration of the Fabrication of G-DHSNs and Its Drug Release Mechanism in Cancer Cell

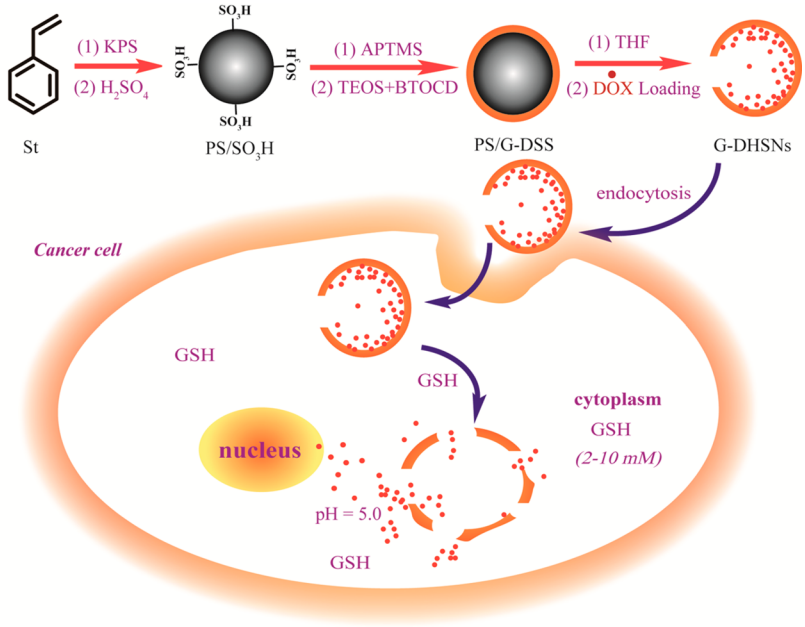

in clinical treatment, and these additional modifications might lead to extra cytotoxicity.

Among the various redox sensitive drug delivery systems, disulfide bond was of great interest because of its instability under the reducing glutathione (GSH). The dramatic difference in the GSH concentrations between intracellular (2−10 mM) and extracellular compartments (2−20 μM) in living cells had recently been utilized as a trigger for the intracellular delivery of cancer therapy drugs.[39] Moreover, the GSH concentration in some cancer cells had been reported to be several times higher than that in the normal cells.[40] The disulfide bonds would be cleaved under the high GSH concentration when the DDS enter the cancer cells, resulting in the intracellular release of the drug molecules, which avoided the premature drug leakage in the extracellular environment. A number of redox-responsive drug delivery systems based on the disulfide bonds had been successfully fabricated.[41−47] However, in stimuli-sensitive DDS, dual and multistimuli responsive nanoparticles had shown unprecedented control over drug delivery and release, such as redox/pH dual-responsive DDS.[48] The pH-response had been well studied due to the different pH values in normal and tumor tissues and lower pH in tumor cells and tissues had been used for selective releasing of anticancer drugs in tumor tissues and cells.

Herein, we synthesized a novel single-hole GSH-responsive degradable HSNs (G-DHSNs) by introducing a kind of disulfide bond bridged silane (BTOCD)[49] to the G-DHSNs for efficient intracellular drug delivery (Scheme 1), which also showed the pH trigger property. By etching the polystyrene (PS) nanospheres core coated with a GSH-responsive degradable silica shell (PS/G-DSS), the single-hole G-DHSNs were successfully prepared. The construction of G-DHSNs DDS was simple and convenient in a biological friendly solvent without any extra pernicious factor. DOX, a classic anticancer drug, was chosen as a model drug to assess the drug loading and releasing behaviors of the carriers. The G-DHSNs DDS carried out the DOX release with simultaneous G-DHSNs decomposition driven by cleaving the disulfide bond via GSH and pH stimulation. These excellent features made the G-DHSNs useful in the biomedical field such as cellular therapeutics, imaging and biosensing.

2. EXPERIMENTAL SECTION

2.1. Reagents and Materials. Styrene (St, 99%), potassium persulfate (KPS, 99.5%), ethanol (C_2H_5OH, 99.7%), sulfuric acid (H_2SO_4, 98%), ammonia solution ($NH_3{\cdot}H_2O$, 25%−28%), and diethyl ether (Et_2O, 99%) were purchased from Tianjin Guangfu Fine Chemical Research Institute (Tianjin, China). Tetrahydrofuran (THF, 99.5%) and triethylamine (TEA, 99%) purchased from Tianjin Chemical Reagent (Tianjin, China) were used after being stirred overnight over CaH_2 and distilled under reduced pressure. Tetraethoxysilane (TEOS, 99.99%), (3-aminopropyl)trimethoxysilane (APTMS, 97%), cystamine dihydrochloride (CADHC, 97%) were supplied by alfa aesar (Tianjin, China). 3-(Triethoxysilyl) propyliso-cyanate (IPTS, 95%) and glutathione (GSH, 98%) were purchased from Aladdin Chemistry Co., Ltd. (Beijing, China). Stroke-physiological saline solution (SPSS, 0.9% NaCl) was obtained from Hunan Kelun Pharmaceutical Co., Ltd. (Hunan, China). Deionized (D.I.) water was prepared from Millipore (Bedford, MA, America). All these reagents were of analytical grades.

2.2. Characterization. Transmission electron microscopy (TEM) micrographs were carried out on a JEM-1200EX TEM (Tykyo, Japan) using the copper grid as the sample holder, operating at an accelerated voltage of 100 kV. Scanning electron microscope (SEM) images of materials were obtained using an S-94 4800 SEM (Hitachi, Japan). The size distribution of materials were determined by dynamic light scattering (DLS) using a BI-200SM (Brookhaven, USA) with angle detection at 90°. The ^{1}H NMR spectrum of the samples were recorded with a JEOL-ECS-400 MHz spectrometer (Tykyo, Japan) using tetramethylsilane as an internal standard at 25 °C. The Fourier transform infrared (FTIR) spectrum were acquired with a Nicolet 20 NEXUS 670 FTIR spectrophotometer (Ramsey, MA, USA) using KBr pellets. Fluorescence spectra were recorded with a RF-5301PC fluorescence spectrometer (Shimadzu, Japan). Thermo gravimetric analysis (TGA) was taken on a STA PT1600 Thermal Analyzer Instruments (Linseis, Germany) with the heating rate of 10 °C min^{-1} under N_2 atmosphere. The cellular images were acquired with a confocal laser scanning microscope (CLSM, ZEISS, LSM 510 Meta, Germany).

2.3. Fabrication of GSH-Responsive Degradable HSNs (G-DHSNs). *2.3.1. Synthesis of Disulfide Bond Bridged Silane BTOCD.* The BTOCD was synthesized according to our previous work.[49] CADHC (0.5 g, 2.25 mmol) and TEA (1 mL) were added with stirring into 40 mL of anhydrous THF. After the mixture was stirred for 1 h, 2 equiv of IPTS (1.2 mL, 4.5 mmol) were added, and the reaction lasted for 24 h. The above experiments were carried at 25 °C. The mixture was then filtered to remove the salt, and the crude product was recovered by evaporation of THF. The resulting product BTOCD was isolated by precipitation in cold diethyl ether, filtration, and drying in vacuo.

2.3.2. Preparation of PS Nanospheres Functionalized with Sulfonic Group (PS/SO_3H). PS/SO_3H particles were prepared according to the ref 50. Monodispersed PS nanospheres were synthesized by surfactant-free emulsion polymerization first. In a typical process, 1.5 mL of St and 150 mL of D.I. water were introduced into a three-neck round-bottom flask equipped with a mechanical stirrer, reflux condenser, nitrogen inlet, and temperature controller. After the mixture was deoxygenated and ultrasonic treated, the flask was placed in a 70 °C oil bath and prepolymerized for 10 min, then followed by adding 0.17 g of KPS (in 5 mL of D.I. water).The reaction was lasted for 6 h at 70 °C. Finally, the PS nanospheres were washed with D.I. water and then collected by centrifugation at 12000 rpm. The obtained PS nanospheres were dispersed in 30 mL of concentrated sulfuric acid to finish the sulfonation reaction at 40 °C for 4 h. The product of PS/SO_3H was obtained by centrifugation at 12000 rpm and washed with D.I. water to remove the residual acid.

2.3.3. Preparation of PS/G-DSS and Etching the PS Core. The obtained PS/SO_3H particles (0.5 g) were directly dispersed in 20 mL of water, and 60 μL of APTMS was added to the mixture under stirring. The reaction between $-SO_3H$ and the $-NH_2$ group was carried out with stirring for 12 h at 25 °C, then, the functionalized nanoparticles were obtained by centrifugation at 12000 rpm for 15 min and washed with ethanol repeatedly.

The above functionalized nanoparticles obtained were dispersed in 35 mL of ethanol and 5 mL of ammonia solution. Then, the mixture was heated to 50 °C, BTOCD (0.15 g, 0.23 mmol) and TEOS (60 μL, 0.27 mmol) were rapidly added under vigorous stirring. After the mixture was stirred at 50 °C for 3 h, the white product was collected by centrifugation at 12000 rpm for 15 min and washed three times with D.I. water.

Next, to remove the PS template, the as-synthesized materials were soaked in 30 mL of THF for 2 h. Finally, G-DHSNs were obtained by centrifugation at 12000 rpm for 15 min and washed five times with D.I. water.

2.4. GSH-Responsive Studies. *2.4.1. Degradation Study of G-DHSNs in Response to GSH.* To estimate the degradation of G-DHSNs in response to GSH, 500 μg of G-DHSNs were dispersed in 5 mL of PBS (50 mM, pH 7.4) with 20 mM GSH and placed in a water bath with gentle shaking at 25 °C. At a predetermined time (6 h, 24 h, 48 h), a drop of the above suspension was taken for TEM measurement. In addition, the suspension was centrifuged at 12000 rpm for 15 min, and the obtained solid was used for SEM measurement.

2.4.2. Drug Loading Capacity, Entrapment Efficiency, and in Vitro Release Studies. DOX was used as a model drug to estimate the drug loading capacity and entrapment efficiency and drug release behaviors of the G-DHSNs DDS. First, 10 mg of G-DHSNs was incubated in 5 mL of 0.9% NaCl buffer containing 2 mg DOX for 24 h in dark at 25 °C. The DOX-loaded G-DHSNs were obtained by centrifugation at 12000 rpm for 15 min and washed by buffer solution to remove free DOX. The fluorescence spectra of supernatants were recorded and the loading capacity and entrapment efficiency of DOX was calculated by the following expressions:

$$\text{drug loading capacity \%} = \frac{\text{amount of DOX in G-DHSNs}}{\text{amount of DOX-loaded G-DHSNs}} \times 100\%$$

$$\text{drug entrapment efficiency \%} = \frac{\text{amount of DOX in G-DHSNs}}{\text{total amount of DOX for loading}} \times 100\%$$

For in vitro drug release, the release studies were performed at 37 °C in phosphate buffer (PBS, 50 mM, pH 7.4 and 5.0) by the dialysis method. First, 5 mg of the DOX-loaded G-DHSNs were dispersed in 5 mL of medium and placed in a dialysis bag (cutoff molecular weight 3500 Da). Then, the dialysis bag was soaked in 45 mL of PBS (50 mM, pH 7.4 and 5.0) with 10 mM GSH in a water bath with gentle shaking. At desired time intervals, 3 mL of release media was taken out and replenished with an equal volume of fresh medium. The control experiment was finished as above with absence of GSH. Finally, the released DOX was estimated by the fluorescent spectrometry signal of DOX (excitation at 488 nm and emission at 586 nm). The drug release studies were performed in triplicate for each of the samples.

2.5. Toxicity Assessment. *2.5.1. Hemolysis Assay of G-DHSNs in Vitro.* The hemolysis assay was carried out according to our previous report with some improvements to evaluate the blood compatibility of G-DHSNs nanocarriers.[51,52] Ethylenediamine tetraacetic acid (EDTA)-stabilized human blood samples were freshly obtained from Gansu Blood Center (Lanzhou, China). First, 3 mL of blood sample was added to 6 mL of isotonic SPSS to separate the serum and red blood cells (RBCs). The RBCs were further washed with 6 mL isotonic SPSS more than five times to ensure the removal of any released hemoglobin and then dispersed in 15 mL of SPSS. The G-DHSNs suspended in isotonic SPSS with different concentrations were prepared immediately before incubation with RBCs. In a typical process, 0.3 mL of the diluted RBCs suspension was mixed with (a) 1.2 mL of D.I. water as the positive control and isotonic SPSS as negative controls; (b) 1.2 mL G-DHSNs at concentrations of 10, 50, 100, 250, and 500 μg/mL. All the sample tubes were kept in static condition at 25 °C for 3 h. Finally, the mixtures were centrifuged and the absorbance values of the supernatants at 575 nm were determined by using UV−visible absorption spectrum. The percent hemolysis of RBCs was calculated using the following formula:

$$\text{hemolysis \%} = \frac{\text{sample absorbance} - \text{negative control absorbance}}{\text{positive control absorbance} - \text{negative control absorbance}} \times 100\%$$

2.5.2. Cell Viability Assay. The cytotoxicities of G-DHSNs and DOX-G-DHSNs nanocarriers were assessed by the MTT assay. The human tongue squamous cell carcinoma TCA8113 cell lines were seeded into a 96-well plate at a density of approximate 3×10^4 cells per well and incubated for 24 h. The cells were then exposed to various concentrations of free DOX, G-DHSNs and DOX-G-DHSNs in culture medium. After treatment for 24 h, the medium was removed from the 96-well plate and 100 μL of 10% trichloroacetic acid were added in for 1 h at 4 °C. Then the wells were gently washed with deionized water and stained with 100 μL of 0.4% Sulforhodamine B (SRB) solution per well for 30 min. After that, 1% acetic acid was used to rinse out unbound SRB. Finally, 150 μL of aqueous tris base (tris(hydroxymethyl)amino-methane) was added in each well. When the SRB dyes were dissolved completely, the spectrophotometrical absorbance was measured on a microplate reader (Huake, Shanghai) at 570 nm. The pure growth medium without treatment of material was used as the negative control.

2.6. Cellular Uptake and Flow Cytometry Studies. For investigation on cell uptake of G-DHSNs nanocarriers, a Confocal laser scanning microscope (CLSM, ZEISS, LSM 510 Meta, Germany) was used for live TCA8113 cell imaging. The human tongue squamous cell carcinoma TCA8113 cells lines were seeded into 6-well plates at densities of 3×10^4 cells/well, and incubated at 37 °C for 24 h. Free DOX and DOX-G-DHSNs at concentration of 5 μg/mL equivalent DOX were added and incubated with TCA8113 cells for 3 and 24 h. 4, 6-diamidino-2-phenylindole (DAPI) (Sigma-Aldrich) was used to stain the cell nucleus. The cells were washed by phosphate buffered saline

(PBS) three times to remove the dead cells and the DAPI adsorbed on the outer surface of the cell membrane. Subsequently, the Free DOX and DOX-G-DHSNs uptake were visualized at 586 nm with an excitation wavelength of 488 nm.

To measure the internalization of DOX quantitatively, the flow cytometry was used for the study. Free DOX and DOX-G-DHSNs at concentration of 5 μg/mL equivalent DOX were added and incubated with TCA8113 cells at 37 °C under 5% CO_2 atmosphere for 3 and 24 h, respectively. The cells were washed with PBS before they were removed from the culture dish with 0.02% EDTA, counted, resuspended in fresh medium. After washing with a solution of PBS, the cells were centrifuged at 450 rpm, and the supernatant was removed. Then the cells resuspended in 500 μL precooling PBS, and analyzed immediately by flow cytometry. The same concentration of G-DHSNs was used as the control.

3. RESULTS AND DISCUSSION

3.1. Formation and Characteristics of G-DHSNs. The fabrication of G-DHSNs was done using PS nanospheres as the sacrificial template and GSH-responsive degradable silica shell as the major structure. The PS nanospheres were chosen as the sacrificial template because they could be prepared with the surfactant-free emulsion polymerization process in which no emulsifiers were used. Besides, hollow structure could be easily fabricated by placing the PS nanospheres in THF, owing to the dissolving of PS nanospheres core. Meanwhile, the PS could swell and burst out through the shell and make a hole on the shell. It was well-known that nanoparticle-based DDS with sizes in the range of 20−200 nm could avoid renal filtration, leading to prolonged residence time in the bloodstream which achieved more effective targeting of diseased tissues by the EPR effect.[53]

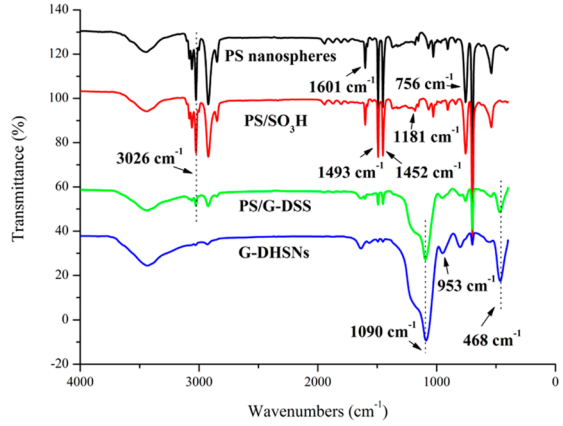

Figure 1. FTIR spectra of PS nanospheres, PS/SO_3H, PS/G-DSS, and G-DHSNs.

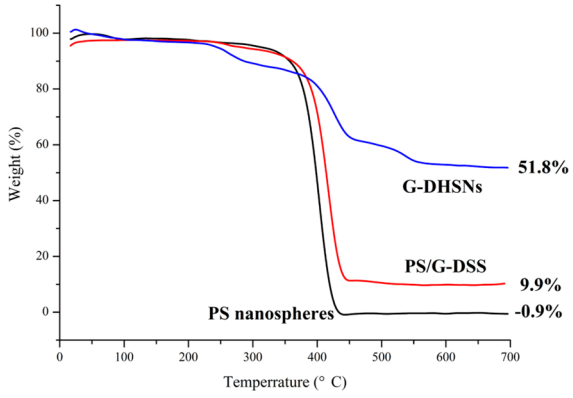

Figure 2. TGA curves of PS nanospheres, PS/G-DSS, and G-DHSNs.

First, BTOCD was successfully synthesized, which was reported in our previous work.[49] The synthetic route and ^{1}HNMR spectrum of the BTOCD were clearly shown in Supporting Information Figure S1. According to the ^{1}HNMR spectrum, the disulfide bond (H^i) and formation of urea (H^g, H^f) in product clearly demonstrated the successful synthesis of the BTOCD. In addition, the FTIR spectrum of BTOCD (Supporting Information Figure S2) showed the characteristic absorption peaks of urea at 1629 cm^{-1}($\nu_{C=O}$), 1588 cm^{-1}(δ_{N-H}), 1440 cm^{-1}(ν_{C-N}), and the asymmetrical stretching vibration of Si−O−C bond was found at 1080 cm^{-1}.

FTIR spectroscopy was employed to further investigate the functional groups and components in the samples, the results are shown in Figure 1. The observed strong FTIR absorption bands at 3026, 1601, 1493, 1452, 756, and 698 cm^{-1} agreed well with the typical PS absorption bands. In the spectrum of PS/SO_3H, the asymmetric stretching vibration of S═O group at 1181 cm^{-1} was observed. The FTIR spectrum of the PS/G-DSS and G-DHSNs revealed characteristic bands associated with Si−O−Si asymmetric stretching at 1090 cm^{-1}, Si−O−Si symmetric vibration at 802 cm^{-1}, and Si−OH stretching at 953 cm^{-1} and bending at 468 cm^{-1}. The typical PS absorption bands were absent in the G-DHSNs spectra, demonstrating that the PS cores were dissolved and removed by THF.

TGA data showed the weights change of PS, PS/G-DSS and G-DHSNs samples during the heat-treatment process (Figure 2). The weight loss stage below 350 °C was attributed to the evaporation of physically adsorbed water and residual solvent in the samples.[54] As shown in Figure 2, a narrow weight-loss stage of PS nanospheres occurred in the region of 348−450 °C, the major weight loss of the PS nanospheres core was completed at 450 °C, whereas the residue of PS/G-DSS remained about 9.9%. It was found that the weight loss of the G-DHSNs was about 48.2%, which was attributed to the decomposition of organic groups in BTOCD. This fact indicated that PS nanospheres core was coated with about 19.1% of GSH-responsive degradable silica shell.

The elemental analysis data was given in Supporting Information Table S1, which also indicated the successful fabrication of PS/SO_3H, PS/G-DSS, and G-DHSNs.

To confirm the morphologies of fabrication of G-DHSNs, the TEM and SEM images of fabrication of G-DHSNs are shown in Figure 3. After a series of optimized conditions, PS nanospheres of an average diameter of 180 ± 5 nm were obtained with good monodispersity (Figure 3a). Next, PS/SO_3H particles were produced (Figure 3b) via sulfonation reaction, which could enhance the deposition of silica shell on the surface of PS nanospheres. As shown in Figure 3b, the average particle diameters of the PS/SO_3H were about 190 ± 5 nm and an obvious sulfonation shell could be observed. To prepare G-DHSNs with a good structure and better drug delivery efficiency, the molar ratio of TEOS and BTOCD was chosen at 1:1. Finally, the G-DHSNs were obtained by removing the PS nanospheres core. Figure 3c-d showed the TEM and SEM images of G-DHSNs. It could be clearly observed that the morphologies of G-DHSNs were predominated with hollow spheres, and the average size was around 200 ± 5 nm. The hole could be clearly seen in the SEM images of G-DHSNs (Figure 3d). The size distributions of PS nanospheres and G-DHSNs were further confirmed by dynamic light scattering (DLS) (Supporting Information Figure S3). It

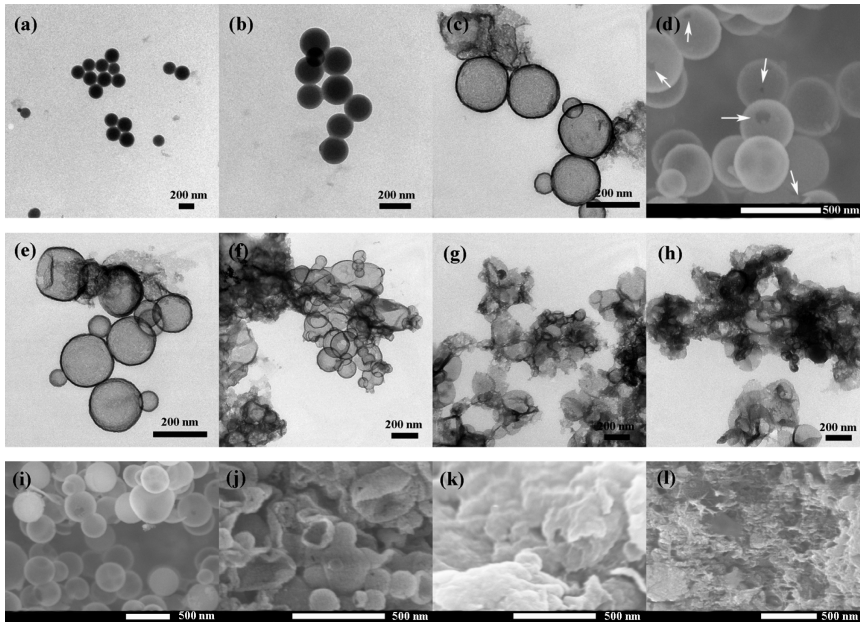

Figure 3. TEM images of (a) PS nanospheres, (b) PS/SO_3H, (c) G-DHSNs, SEM images of (d) G-DHSNs; TEM images (e, f, g, h), and SEM images (i, j, k, l) of G-DHSNs incubated with PBS (50 mM, pH 7.4) containing 20 mM GSH for 0 (e, (i), 6 (f, j), 24 (g, k), 48 h (h, l).

Scheme 2. Degradation Process of G-DHSNs in Response to GSH

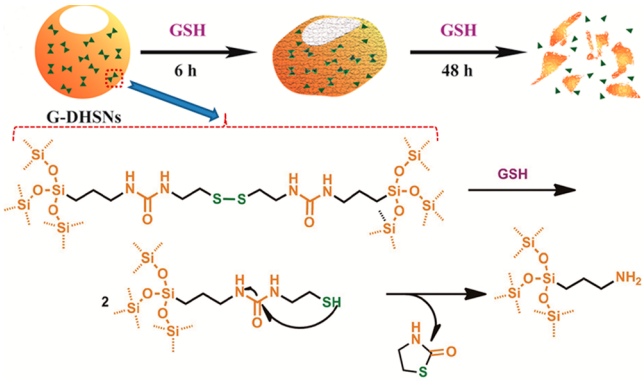

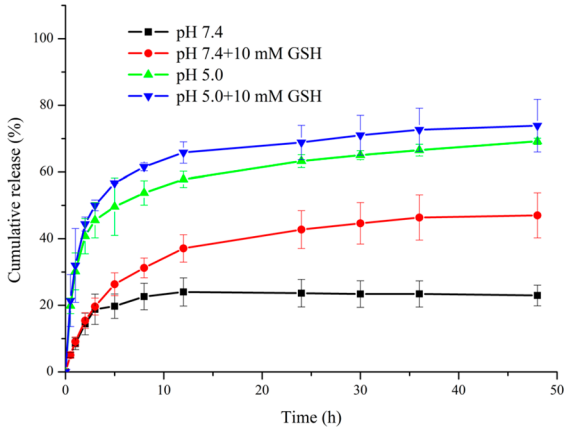

Figure 4. Time course of DOX release from DOX-G-DHSNs at 37 °C at pH 5.0 or 7.4 in the presence or absence of 10 mM GSH. Released DOX was separated by dialysis and quantified by spectrophotometer.

must be noted that THF was not a biocompatibility reagent, but it could be easily removed by D.I. water due to its excellent

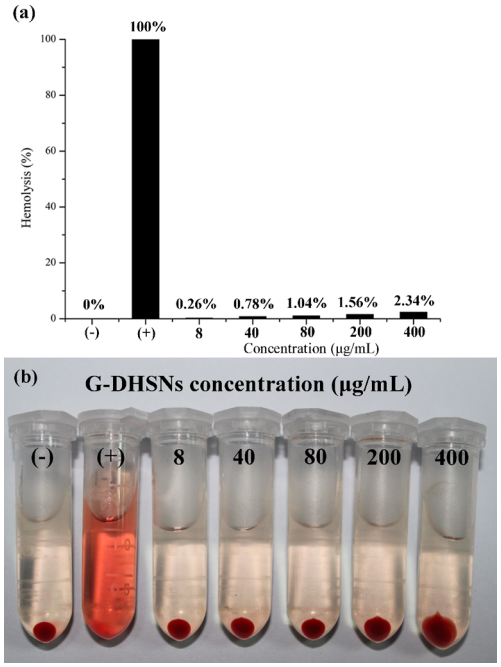

Figure 5. (a) The hemolysis percentages of G-DHSNs in SPSS at concentrations of 8, 40, 80, 200, and 400 μg/mL; isotonic SPSS as negative control (−) and D.I. water as positive control (+). (b) Photograph of hemolysis assay to detect the presence of hemoglobin in the supernatant of G-DHSNs in SPSS at above concentrations.

water-solubility. In all, such a surfactant-free nanoparticle without any extra pernicious functionalization should be advantageous for many clinical practices and potential development.

3.2. Degradation Study of G-DHSNs. On the basis of our design, the disulfide bond would be widely distributed in the structure of G-DHSNs, due to the introduction of the BTOCD in the preparation process of G-DHSNs. As mentioned earlier, the disulfide linkage could be cloven by GSH. Furthermore, the

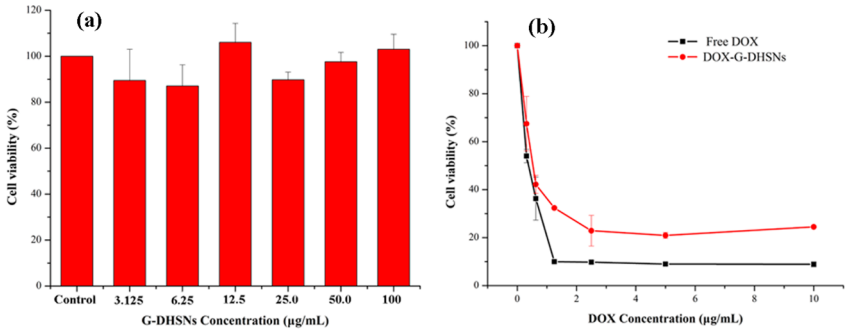

Figure 6. Relative cell viabilities of TCA8113 cells incubated with different concentrations of (a) G-DHSNs and (b) free DOX and DOX-G-DHSNs for 24 h.

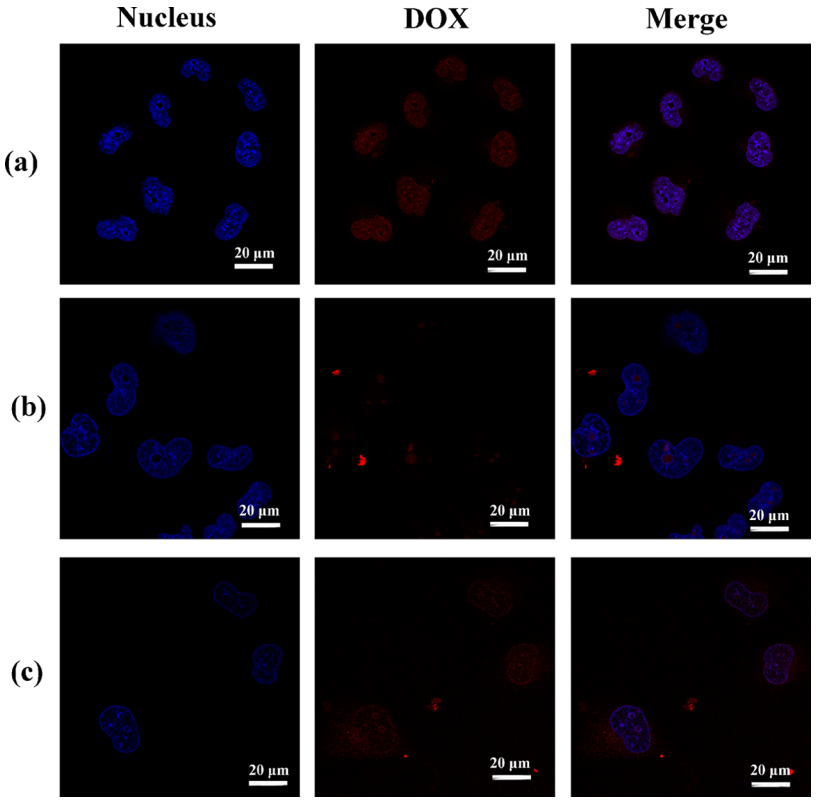

Figure 7. CLSM images of TCA8113 cells incubated with free DOX and DOX-G-DHSNs. For each panel, the images from left to right show DOX fluorescence in cell nuclei stained by DAPI (blue), cells (red), and overlays of the two images. (a) Free DOX, 3 h incubation; (b) DOX-G-DHSNs, 3 h incubation; (c) DOX-G-DHSNs, 24 h incubation.

disulfide bond cleavage was expected to be followed by intramolecular cyclization and cleavage of the neighboring amide bond, which led to the degradation of G-DHSNs (Scheme2). To investigate the release mechanism, especially under stimulus, the degradation study of G-DHSNs was carried out. The corresponding decomposition of the G-DHSNs in response to GSH was illustrated by the morphological evolution of G-DHSNs using TEM and SEM images taken as a function of time (Figure 3). The G-DHSNs were immersed in PBS (50 mM, pH 7.4) with 20 mM GSH for specified period of times (6 h, 24 h, 48 h) at room temperature. The corresponding morphological evolutions of G-DHSNs were observed. After 48 h in PBS (50 mM, pH 7.4) without GSH, the morphology of G-DHSNs (Supporting Information Figure S4) presented a negligible change. By contrast, as shown in Figure 3e–h and Figure 3i–l, one could observe that the hollow feature started partly broken in the early time, and eventually leading to complete fragmentation of the G-DHSNs. The above experimental results suggested possible control over the drug release with simultaneously carrier decomposition, which was driven by breaking the disulfide bond in the G-DHSNs via GSH.

3.3. Drug Loading and in Vitro Release Studies. DOX was used as a model drug because of its inherent fluorescence. Through measurement and calculation, the DOX loading capacity was 14 ± 3.2% and 78 ± 6.5% DOX was effectively encapsulated into the G-DHSNs, The relatively high loading capacity in the current study was assumed to be a result of the hollow structure and the hole of G-DHSNs.

Then, the release of DOX from DOX-loaded G-DHSNs in response to GSH and pH was investigated in PBS buffer (pH 7.4 and 5.0) in the presence or absence of 10 mM GSH. Figure 4 showed the significant dependence of DOX cumulative release upon GSH, and pH also played an important role in the

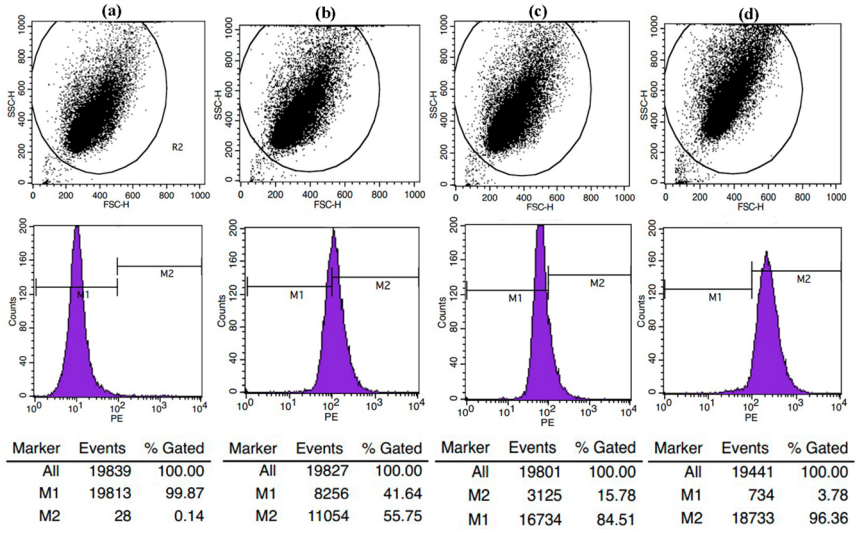

Marker	Events	% Gated
All	19839	100.00
M1	19813	99.87
M2	28	0.14

Marker	Events	% Gated
All	19827	100.00
M1	8256	41.64
M2	11054	55.75

Marker	Events	% Gated
All	19801	100.00
M2	3125	15.78
M1	16734	84.51

Marker	Events	% Gated
All	19441	100.00
M1	734	3.78
M2	18733	96.36

Figure 8. Penetration of DOX into cells measured by flow cytometry after TCA8113 cells incubated with (a) control; (b) free DOX, 3 h; (c) DOX-G-DHSNs, 3 h; (d) DOX-G-DHSNs, 24 h. Dot-plot of cells forw and light scatter (FSC) and side light scatter (SSC) (top), the distribution of fluorescence intensities of cells (middle, bottom). M1, negative cells; M2, positive cells.

release of DOX. At pH 7.4 without the presence of GSH, only about 23% of DOX in the DOX-loaded G-DHSNs was released in 48 h. By contrast, it was found that the drug release was significantly enhanced by addition of 10 mM GSH, the cumulative release of DOX was more than twice over that with absence of GSH. The release of DOX was also boosted under a simulating tumor environment containing 10 mM GSH at pH 5.0, in which 74% of DOX was released in 48 h. These results clearly indicated that G-DHSNs presented GSH and pH double effect in drug release. However, the above release properties were favorable for enhanced DOX accumulation in the cytoplasm of cancer cells following endocytosis and reduced DOX release from the DOX-loaded G-DHSNs in normal tissue.

3.4. Hemolytic Activity Assay. The hemolytic activity assay was used to study the cytotoxic effect of G-DHSNs on human RBCs so as to evaluate the blood compatibility of G-DHSNs under physiological conditions. Hemolysis was evaluated by measuring the amount of hemoglobin released in the supernatant from the RBCs incubation with isotonic SPSS containing the materials studied at room temperature for 3 h. (Figure 5a). As shown in photographs of hemolysis of RBCs (Figure 5b), the positive control showed a significantly higher hemoglobin release than others, due to the destroying of cell membrane. Nevertheless, the G-DHSNs sample even at the high concentration of 400 μg/mL indicated a significantly low hemoglobin release. The hemolytic activity as low as 2.34 $\pm$ 0.79%, which could promote the application of G-DHSNs DDS in vivo when administered intravenously in the broad concentration range of 0−400 μg/mL.

3.5. Cell Viability Assay, Cellular Uptake, and Flow Cytometry Studies. MTT assay was used to investigate the TCA8113cell viability of free DOX, G-DHSNs, and DOX-G-DHSNs after 24 h incubation. As shown in Figure 6a, the G-DHSNs were found to be noncytotoxicity for TCA8113 cells (cell viability above 87%) in the concentration range 3.125−100 μg/mL, which exhibited excellent biocompatibility. Once DOX was loaded, cell death of DOX-G-DHSNs group nearly caught that of free DOX, cell-killing ratio was about 75.5% at the drug concentration of 10.0 μg/mL (Figure 6b). The DOX-G-DHSNs, upon uptake by cells, the loaded DOX would be released in cytoplasm because of the higher concentration of GSH, and thereby inhibit TCA8113 cells growth.

Because of the inherent fluorescence properties of DOX, the intracellular delivery of DOX was possible by observing CLSM images of TCA8113 cells treated with free DOX and DOX-G-DHSNs after incubation for 3 and 24 h, respectively. The CLSM results are shown in Figure 7. Obviously, the red fluorescence was from free DOX or DOX-G-DHSNs, and the blue fluorescence was from DAPI-stained cell nuclei. Compared to free DOX as a control (Figure 7a), the images from DOX fluorescence suggested that DOX-G-DHSNs were internalized and DOX was released to reach cell nuclei within 24 h (Figure 7c). The stronger DOX fluorescence was observed in TCA8113 cells following incubation with free DOX for 3 h, for the fast passive diffusion of DOX. However, as shown in Figure 7b, after incubation with DOX-G-DHSNs for 3 h, no obvious red fluorescence could be detected. In such a short time period, it was difficult for the materials to go through a whole procedure of endocytosis. These results confirmed that DOX-G-DHSNs were able to deliver and release DOX into the nuclei of cancer cells.

To investigate the cellular uptake of DOX in the cells quantitatively, the penetration of DOX into cells were measured by flow cytometry after TCA8113 cells were incubated with free DOX and DOX-G-DHSNs. The longer uptake time of DOX-G-DHSNs increased the fluorescence intensity and the ratio of fluorescence-positive cells (M2) (Figure 8c−d). These flow cytometry results were consistent with the CLSM results.

4. CONCLUSION

In summary, we had reported a type of intelligent material G-DHSNs for drug delivery in cancer cells, which exhibited an efficient cancer-targeted intracellular controlled release of the drug. G-DHSNs exhibited excellent colloidal stability, good biocompatibility, and accessible hollow structure. Antineoplastic drug DOX could be effectively loaded in G-DHSNs, the loading efficiency of DOX was approximately 14 $\pm$ 3.2%. In vitro cell viability assay results indicated that DOX-G-DHSNs

could efficient inhibit TCA8113 cells growth. The cellular uptake studies showed that the DOX-G-DHSNs were able to deliver and release DOX into the nuclei of TCA8113 cells because of the increased GSH concentration and lower pH. As a novel biomaterial, the G-DHSNs were expected to be useful for controlled drug delivery.

■ ASSOCIATED CONTENT

Supporting Information

Synthetic route and ^{1}H NMR spectrum of BTOCD, FTIR spectra of BTOCD, the elemental analysis data of PS/SO_3H, PS/G-DSS, and G-DHSNs, DLS data of PS and G-DHSNs nanospheres, and the SEM images of the control in degradation study. This material is available free of charge via the Internet at http://pubs.acs.org.

■ AUTHOR INFORMATION

Corresponding Author

*Tel.: +86 931 8912510. Fax: +86 931 8912582. E-mail: zhanghx@lzu.edu.cn.

Notes

The authors declare no competing financial interest.

■ ACKNOWLEDGMENTS

The authors thank the supporting of National Science Foundation (no. 21375052).

■ REFERENCES

(1) Zhang, Y.; Chan, H. F.; Leong, K. W. Advanced Materials and Processing for Drug Delivery: The Past and the Future. *Adv. Drug Delivery Rev.* **2013**, *65*, 104−120.

(2) Yang, P.; Gai, S.; Lin, J. Functionalized Mesoporous Silica Materials for Controlled Drug Delivery. *Chem. Soc. Rev.* **2012**, *41*, 3679−3698.

(3) Mai, W. X.; Meng, H. Mesoporous Silica Nanoparticles: A Multifunctional Nano Therapeutic System. *Integr. Biol.* **2013**, *5*, 19−28.

(4) Zhang, S.; Chu, Z.; Yin, C.; Zhang, C.; Lin, G.; Li, Q. Controllable Drug Release and Simultaneously Carrier Decomposition of SiO_2-Drug Composite Nanoparticles. *J. Am. Chem. Soc.* **2013**, *135*, 5709−5716.

(5) Kim, B. H.; Kim, S.; Park, C.; Lee, H.; Park, H. J.; Kim, C. Glutathione-Induced Intracellular Release of Guests from Mesoporous Silica Nanocontainers with Cyclodextrin Gatekeepers. *Adv. Mater.* **2010**, *22*, 4280−4283.

(6) Feng, J.; Su, W.; Wang, H.; Huang, F.; Zhang, X.; Zhuo, R. Facile Fabrication of Diblock Methoxy Polyethylene glycol)-poly-(trimethylene carbonate) and Its Self-Assembled Micelles as Drug Carriers. *ACS Appl. Mater. Interfaces* **2009**, *12*, 2729−2737.

(7) Babiuch, K.; Gottschaldt, M.; Werz, O.; Schubert, U. S. Particulate Transepithelial Drug Carriers: Barriers and Functional Polymers. *RSC Adv.* **2012**, *2*, 10427−10465.

(8) Ha, C. S.; Gardella, J. A. Surface Chemistry of Biodegradable Polymers for Drug Delivery Systems. *Chem. Rev.* **2005**, *105*, 4205−4232.

(9) Bagalkot, V.; Zhang, L.; Levy-Nissenbaum, E.; Jon, S.; Kantoff, P. W.; Farokhzad, O. C. Quantum Dot-Aptamer Conjugates for Synchronous Cancer Imaging, Therapy, and Sensing of Drug Delivery Based on Bi-Fluorescence Resonance Energy Transfer. *Nano Lett.* **2007**, *7*, 3065−3070.

(10) Hu, J.; Wu, T.; Zhang, G.; Liu, S. Efficient Synthesis of Single Gold Nanoparticle Hybrid Amphiphilic Triblock Copolymers and Their Controlled Self-Assembly. *J. Am. Chem. Soc.* **2012**, *134*, 7624−7627.

(11) Chen, T.; Xu, S.; Zhao, T.; Zhu, L.; Wei, D.; Li, Y.; Zhang, H.; Zhao, C. Gold Nanocluster-Conjugated Amphiphilic Block Copolymer for Tumor-Targeted Drug Delivery. *ACS Appl. Mater. Interfaces* **2012**, *4*, 5766−5774.

(12) Shi, P.; Qu, K.; Wang, J.; Li, M.; Ren, J.; Qu, X. pH-Responsive NIR Enhanced Drug Release from Gold Nanocages Possesses High Potency Against Cancer Cells. *Chem. Commun.* **2012**, *48*, 7640−7642.

(13) Mikhaylov, G.; Mikac, U.; Magaeva, A. A.; Itin, V. I.; Naiden, E. P.; Psakhye, I.; Babes, L.; Reinheckel, T.; Peters, C.; Zeiser, R.; Bogyo, M.; Turk, V.; Psakhye, S. G.; Turk, B.; Vasiljeva, O. Ferri-Liposomes as an MRI-Visible Drug-Delivery System for Targeting Tumours and Their Microenvironment. *Nat. Nanotechnol.* **2011**, *6*, 594−602.

(14) Lee, S. F.; Zhu, X. M.; Wang, Y. X. J.; Xuan, S. H.; You, Q.; Chan, W. H.; Wong, C. H.; Wang, F.; Yu, J. C.; Cheng, C. H. K.; K. Leung, C. F. Ultrasound, pH, and Magnetically Responsive Crown-Ether-Coated Core/Shell Nanoparticles as Drug Encapsulation and Release Systems. *ACS Appl. Mater. Interfaces* **2013**, *5*, 1566−1574.

(15) Yang, K.; Feng, L.; Shi, X.; Liu, Z. Nano-Graphene in Biomedicine: Theranostic Applications. *Chem. Soc. Rev.* **2013**, *42*, 530−547.

(16) Cheng, C.; Nie, S.; Li, S.; Peng, H.; Yang, H.; Ma, L.; Sun, S.; Zhao, C. Biopolymer Functionalized Reduced Graphene Oxide with Enhanced Biocompatibility via Mussel Inspired Coatings/Anchors. *J. Mater. Chem. B* **2013**, *1*, 265−275.

(17) Joseph, D.; Tyagi, N.; Ghimire, A.; Geckeler, K. E. A Direct Route Towards Preparing pH-Sensitive Graphene Nanosheets with Anti-Cancer Activity. *RSC Adv.* **2014**, *4*, 4085−4093.

(18) Matsumura, Y.; Maeda, H. A New Concept for Macromolecular Therapeutics in Cancer Chemotherapy: Mechanism of Tumoritropic Accumulation of Proteins and the Antitumor aAgent Smancs. *Cancer Res.* **1986**, *46*, 6387−6392.

(19) Maeda, H.; Matsumura, Y. Tumoritropic and Lymphotropic Principles of Macromolecular Drugs. *Crit. Rev. Ther. Drug Carrier Syst.* **1988**, *6*, 193−210.

(20) Heurtault, B.; Saulnier, P.; Pech, B.; Proust, J.-E.; Benoit, J.-P. Physico-Chemical Stability of Colloidal Lipid Particles. *Biomaterials* **2003**, *24*, 4283−4300.

(21) Khan, D. R.; Rezler, E. M.; Lauer-Fields, J.; Fields, G. B. Effects of Drug Hydrophobicity on Liposomal Stability. *Chem. Biol. Drug Des.* **2008**, *71*, 3−7.

(22) Amstad, E.; Reimhult, E. Nanoparticle Actuated Hollow Drug Delivery Vehicles. *Nanomedicine* **2012**, *7*, 145−164.

(23) Kong, S. D.; Sartor, M.; Jack Hu, C.-M.; Zhang, W.; Zhang, L.; Jin, S. Magnetic Field Activated Lipid-Polymer Hybrid Nanoparticles for Stimuli-Responsive Drug Release. *Acta Biomater.* **2013**, *9*, 5447−5452.

(24) Chen, N.; He, Y.; Su, Y.; Li, X.; Huang, Q.; Wang, H.; Zhang, X.; Tai, R.; Fan, C. The Cytotoxicity of Cadmium-Based Quantum Dots. *Biomaterials* **2012**, *33*, 1238−1244.

(25) Rzigalinski, B. A.; Strobl, J. S. Cadmium-Containing Nanoparticles: Perspectives on Pharmacology and Toxicology of Quantum Dots. *Toxicol. Appl. Pharmacol.* **2009**, *238*, 280−288.

(26) Chen, Y.; Chen, H.; Ma, M.; Chen, F.; Guo, L.; Zhang, L.; Shi, J. Double Mesoporous Silica Shelled Spherical/Ellipsoidal Nanostructures: Synthesis and Hydrophilic/Hydrophobic Anticancer Drug Delivery. *J. Mater. Chem.* **2011**, *21*, 5290−5298.

(27) Yang, P.; Gai, S.; Lin, J. Functionalized Mesoporous Silica Materials for Controlled Drug Delivery. *Chem. Soc. Rev.* **2012**, *41*, 3679−3698.

(28) Luo, Z.; Ding, X.; Hu, Y.; Wu, S.; Xiang, Y.; Zeng, Y.; Zhang, B.; Yan, H.; Zhang, H.; Zhu, L.; Liu, J.; Li, J.; Cai, K.; Zhao, Y. Engineering a Hollow Nanocontainer Platform with Multifunctional Molecular Machines for Tumor-Targeted Therapy in Vitro and in Vivo. *ACS Nano* **2013**, *7*, 10271−10284.

(29) Shi, S.; Chen, F.; Cai, W. Biomedical Applications of Functionalized Hollow Mesoporous Silica Nanoparticles: Focusing on Molecular Imaging. *Nanomedicine* **2013**, *8*, 2027−2039.

(30) Shen, J.; Song, G.; An, M.; Li, X.; Wu, N.; Ruan, K.; Hu, J.; Hu, R. The Use of Hollow Mesoporous Silica Nanospheres to Encapsulate Bortezomib and Improve Efficacy for Non-Small Cell Lung Cancer Therapy. *Biomaterials* **2014**, *35*, 316−326.

(31) Ma, X.; Zhao, Y.; Ng, K. W.; Zhao, Y. Integrated Hollow Mesoporous Silica Nanoparticles for Target Drug/siRNA Co-Delivery. *Chem.—Eur. J.* **2013**, *19*, 15593−15603.
(32) Du, L.; Liao, S.; Khatib, H. A.; Stoddart, J. F.; Zink, J. I. Controlled-Access Hollow Mechanized Silica Nanocontainers. *J. Am. Chem. Soc.* **2009**, *131*, 15136−15142.
(33) Bang, A.; Sadekar, A. G.; Buback, C.; Curtin, B.; Acar, S.; Kolasinac, D.; Yin, W.; Rubenstein, D. A.; Lu, H.; Leventis, N.; Sotiriou-Leventis, C. Evaluation of Dysprosia Aerogels as Drug Delivery Systems: A Comparative Study with Random and Ordered Mesoporous Silicas. *ACS Appl. Mater. Interfaces* **2014**, *6*, 4891−4902.
(34) Liu, T.; Li, L.; Teng, X.; Huang, X.; Liu, H.; Chen, D.; Ren, J.; He, J.; Tang, F. Single and Repeated Dose Toxicity of Mesoporous Hollow Silica Nanoparticles in Intravenously Exposed Mice. *Biomaterials* **2011**, *32*, 1657−1668.
(35) Lai, C.-Y.; Trewyn, B. G.; Jeftinija, D. M.; Jeftinija, K.; Xu, S.; Jeftinija, S.; Lin, V. S.-Y. A Mesoporous Silica Nanosphere-Based Carrier System with Chemically Removable CdS Nanoparticle Caps for Stimuli-Responsive Controlled Release of Neurotransmitters and Drug Molecules. *J. Am. Chem. Soc.* **2003**, *125*, 4451−4459.
(36) Lovric, J.; Cho, S. J.; Winnik, F. M.; Maysinger, D. Unmodified Cadmium Telluride Quantum Dots Induce Reactive Oxygen Species Formation Leading to Multiple Organelle Damage and Cell Death. *Chem. Biol.* **2005**, *12*, 1227−1234.
(37) Chan, W.; Shiao, N. Cytotoxic Effect of CdSe Quantum Dots on Mouse Embryonic Development. *Acta Pharmacol. Sin.* **2008**, *28*, 259−266.
(38) Zhu, Y.; Meng, W.; Gao, H.; Hanagata, N. Hollow Mesoporous Silica/Poly(L-lysine) Particles for Codelivery of Drug and Gene with Enzyme-Triggered Release Property. *J. Phys. Chem. C* **2011**, *115*, 13630−13636.
(39) Navath, R. S.; Kurtoglu, Y. E.; Wang, B.; Kannan, S.; Romero, R.; Kannan, R. M. Dendrimer−Drug Conjugates for Tailored Intracellular Drug Release Based on Glutathione Levels. *Bioconjugate Chem.* **2008**, *19*, 2446−2455.
(40) Russo, A.; Degraff, W.; Friedman, N.; Mitchell, J. B. Selective Modulation of Glutathione Levels in Human Normal versus Tumor Cells and Subsequent Differential Response to Chemotherapy Drugs. *Cancer Res.* **1986**, *46*, 2845−2848.
(41) Bauhuber, B. S.; Hozsa, C.; Breunig, M.; Göpferich, A. Delivery of Nucleic Acids via Disulfide-Based Carrier Systems. *Adv. Mater.* **2009**, *21*, 3286−3306.
(42) Muniesa, C.; Vicente, V.; Quesada, M.; Sáez-Atiénzar, S.; Blesa, J. R.; Abasolo, I.; Fernández, Y.; Botella, P. Glutathione-Sensitive Nanoplatform for Monitored Intracellular Delivery and Controlled Release of Camptothecin. *RSC Adv.* **2013**, *3*, 15121−15131.
(43) Hong, R.; Han, G.; Fernández, J. M.; Kim, B.; Forbes, N. S.; Rotello, V. M. Glutathione-Mediated Delivery and Release Using Monolayer Protected Nanoparticle Carriers. *J. Am. Chem. Soc.* **2006**, *128*, 1078−1079.
(44) Kim, B. H.; Kim, S.; Park, C.; Lee, H.; Park, H. J.; Kim, C. Glutathione-Induced Intracellular Release of Guests from Mesoporous Silica Nanocontainers with Cyclodextrin Gatekeepers. *Adv. Mater.* **2010**, *22*, 4280−4283.
(45) Meng, F.; Hennink, W. E.; Zhong, Z. Reduction-Sensitive Polymers and Bioconjugates for Biomedical Applications. *Biomaterials* **2009**, *30*, 2180−2198.
(46) Huo, M.; Yuan, J.; Tao, L.; Wei, Y. Redox-Responsive Polymers for Drug Delivery: From Molecular Design to Applications. *Polym. Chem.* **2014**, *5*, 1519−1528.
(47) Xu, Z.; Wang, D.; Xu, S.; Liu, X.; Zhang, X.; Zhang, H. Preparation of a Camptothecin Prodrug with Glutathione-Responsive Disulfide Linker for Anticancer Drug Delivery. *Chem.—Asian J.* **2014**, *9*, 199−205.
(48) Chen, W.; Zhong, P.; Meng, F.; Cheng, R.; Deng, C.; Feijen, J.; Zhong, Z. Redox and pH-Responsive Degradable Micelles for Dually Activated Intracellular Anticancer Drug Release. *J. Controlled Release* **2013**, *169*, 171−179.
(49) Xu, Z.; Zhang, K.; Liu, X.; Zhang, H. A New Strategy to Prepare Glutathione Responsive Silica Nanoparticles. *RSC Adv.* **2013**, *3*, 17700−17702.
(50) Feng, X.; Mao, C.; Yang, G.; Hou, W.; Zhu, J. J. Polyaniline/Au Composite Hollow Spheres: Synthesis, Characterization, and Application to the Detection of Dopamine. *Langmuir* **2006**, *22*, 4384−4389.
(51) Xu, Z.; Wang, D.; Guan, M.; Liu, X.; Yang, Y.; Wei, D.; Zhao, C.; Zhang, H. Photoluminescent Silicon Nanocrystal-Based Multifunctional Carrier for pH-Regulated Drug Delivery. *ACS Appl. Mater. Interfaces* **2012**, *4*, 3424−3431.
(52) Roggers, R. A.; Joglekar, M.; Valenstein, J. S.; Trewyn, B. G. Mimicking Red Blood Cell Lipid Membrane To Enhance the Hemocompatibility of Large-Pore Mesoporous Silica. *ACS Appl. Mater. Interfaces* **2014**, *6*, 1675−1681.
(53) Park, J. H.; Gu, L.; von Maltzahn, G.; Ruoslahti, E.; Bhatia, S. N.; Sailor, M. J. Biodegradable Luminescent Porous Silicon Nanoparticles For in Vivo Applications. *Nat. Mater.* **2009**, *8*, 331−336.
(54) Zou, H.; Wu, S.; Shen, J. Preparation of Silica-Coated Poly(Styrene-co-4-vinylpyridine) Particles and Hollow Particles. *Langmuir* **2008**, *24*, 10453−10461.